

The thickness and internal structure of Fireweed rock glacier, Alaska, U.S.A., as determined by geophysical methods

ADAM K. BUCKI,¹ KEITH A. ECHELMMEYER,¹ SCOTT MACINNES²

¹*Geophysical Institute, University of Alaska, 903 Koyukuk Drive, Fairbanks, Alaska 99775-7320, U.S.A.*

E-mail: akbucki@gi.alaska.edu

²*Zonge Engineering, 37029 Denise Lake Drive, Soldotna, Alaska 99669, U.S.A.*

ABSTRACT. Geophysical investigations on rock glaciers are often difficult because rock glaciers are covered by an unconsolidated debris mantle a few meters thick, are typically <50 m thick and are composed of an ice–rock mixture of unknown composition. Transient electromagnetics (TEM) is a method that allows some of these difficulties to be minimized, and data collection is relatively efficient. TEM, with calibration from terminus exposure, was used to determine the thickness (~60 m) of Fireweed rock glacier, Alaska, U.S.A., under complex valley geometry. A conductive layer beneath the rock glacier was identified, and its distribution is consistent with a till-like layer. Seismic refraction, used to resolve the debris-mantle thickness (2–4 m), suggests the presence of a discontinuity at 18–28 m depth within the rock glacier. The discontinuity is also indicated in the radio-echo sounding and the TEM data, but to a lesser extent. This discontinuity is important because the motion of the rock glacier may occur across this as a “shear plane”.

INTRODUCTION

Estimates of the thickness and cross-sectional shape of a rock glacier are important for understanding its stress distribution and motion. On ice glaciers this geometry is routinely determined using seismic and ice-radar methods. These methods are difficult to apply to rock glaciers because rock glaciers are thinner, are composed of a mixture of ice and rock of unknown composition and are covered by a 2–3 m thick layer of unconsolidated rock (the “debris mantle”). Radio-echo sounding (RES) is difficult because the absorption and scattering of radar waves are stronger in rock-glacier ice–rock mixtures than in clean ice (Haeberli, 1985) and the basal interface may not be distinct. However, Berthling and others (2000), Degenhardt and others (2000), Isaksen and others (2000), Vonder Mühlh and others (2001) and Degenhardt and Giardino (2003) were successful in using ground-penetrating radar (GPR) to discern the basal interface and/or internal structures of some rock glaciers. Seismic methods are complicated by the debris mantle, which limits the transfer energy from the source (usually an explosion) into the rock glacier and inhibits geophone coupling. Seismic field techniques have been devised to overcome these problems (Costello, 2000), but are difficult to apply on a routine basis and have shown limited success. Direct-current (d.c.) electrical resistivity has been widely used in rock-glacier soundings (Fisch and others, 1977; Evin and others, 1997; Hauck, 2001), but the debris mantle again poses problems with electrical coupling and requires labor-intensive field set-ups. We have used all of these methods, with the exception of GPR, to investigate the geometry of Fireweed rock glacier with limited success. We have found that transient electromagnetic (TEM) methods provide the best means of investigating the internal structure and thickness distribution of the rock glacier. TEM methods do

not require a high degree of physical or electrical coupling with the surface substrate. Here we discuss the methods and results for each of the techniques that were applied to Fireweed rock glacier.

DESCRIPTION AND GEOLOGIC SETTING

Fireweed rock glacier is 2 km long and flows down a steep, narrow valley on Fireweed Mountain, which is located in the Wrangell Mountains of south-central Alaska, U.S.A. (61.45° N, 143.08° W; see Fig. 1 and Bucki and Echelmeyer, 2004, fig. 1). This is an active rock glacier (Elconin and LaChapelle, 1997) that emanates from three separate cirques as independent tributaries, each having average surface slopes of about 15°. These tributaries coalesce to form the main trunk that extends 500 m and terminates at a quasi-periodically calving toe (Elconin and LaChapelle, 1997). Surface velocities on the main trunk are up to 3.5 m a⁻¹ (Bucki and Echelmeyer, 2004), which is relatively high compared to other rock glaciers (~2 m a⁻¹; Käab and others, 1997; Konrad and Humphrey, 2000). Within the main trunk, each tributary remains lithologically distinct, forming the east, middle and west flows. There are V-shaped longitudinal troughs between the flows that give the rock-glacier main trunk an irregular transverse topographic profile. The longitudinal profile of the main trunk is much smoother and has an average slope of 11°.

The rock glacier occupies a cirque and valley complex that likely contained a small ice glacier in the past, as indicated by the overall U-shape of the valley. The lower portion of the main trunk fills a narrower V-shaped section that has been eroded into the bottom of the larger U-shaped valley. The main trunk narrows from 240 m in the upper portion to 90 m at the terminus, and the walls of the valley

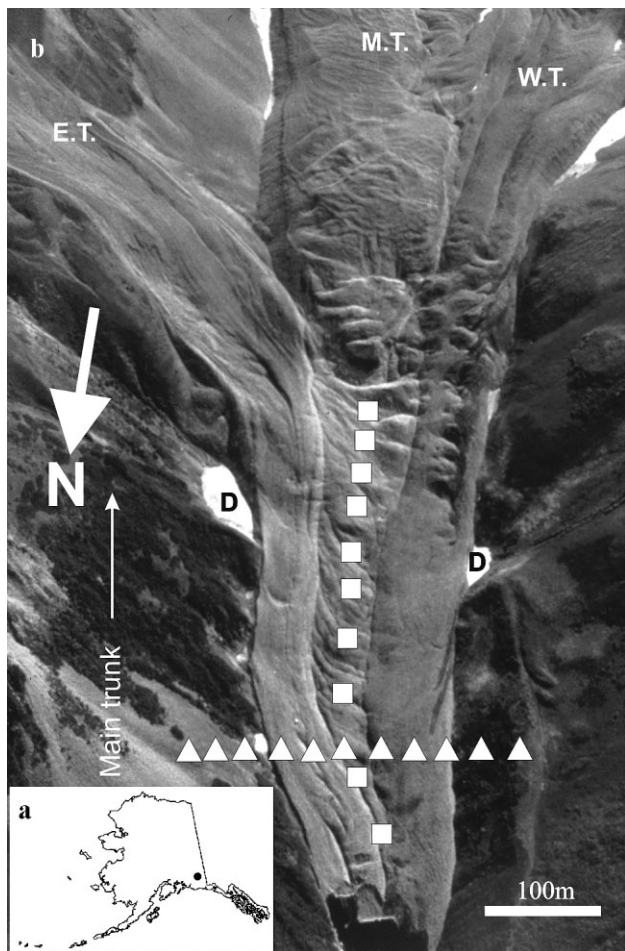


Fig. 1. (a) Location of Fireweed rock glacier in Alaska. (b) Main trunk of the rock glacier showing the east, middle and west tributaries labeled with “E.T.,” “M.T.” and “W.T.” White squares indicate approximate location of individual center-line TEM soundings, whereas triangles mark the path of the transverse soundings. “D” marks the location of marginal, snow-filled depressions corresponding to detected subsurface topography of the rock glacier, about 340 m from terminus.

immediately above the rock-glacier surface have slopes of 25–45°. Extrapolation of these slopes beneath the rock glacier suggests that the main-trunk valley is at least 40–50 m deep along the center line. The terminus face has a slope of 38° and has a center-line thickness of 58 m (Bucki and Echelmeyer, 2004). This face is about 90 m wide at the top and narrows to about 10–15 m at the base, where a periglacial stream emanates.

Fireweed Mountain is the exposed portion of a shallow pluton of Tertiary age that invaded Cretaceous sediments with fine- to medium-grain felsic porphyry dikes and sills. Some of these intrusives are hydrothermally altered, with fine-grained pyrite crystals and centimeter-size feldspar crystals. The sedimentary rocks are mostly mudstones with a few thin beds of limestone; some of these are also hydrothermally altered. The main trunk of the rock glacier flows along a contact between altered and non-altered mudstone (MacKevett and Smith, 1972). The bedrock adjacent to the main trunk does not contribute material to the rock-glacier surface (as indicated by the moderately vegetated margins; Fig. 1); instead the debris is derived from talus cones in the cirques and along the upper portions of the tributaries (Elconin and LaChapelle, 1997).

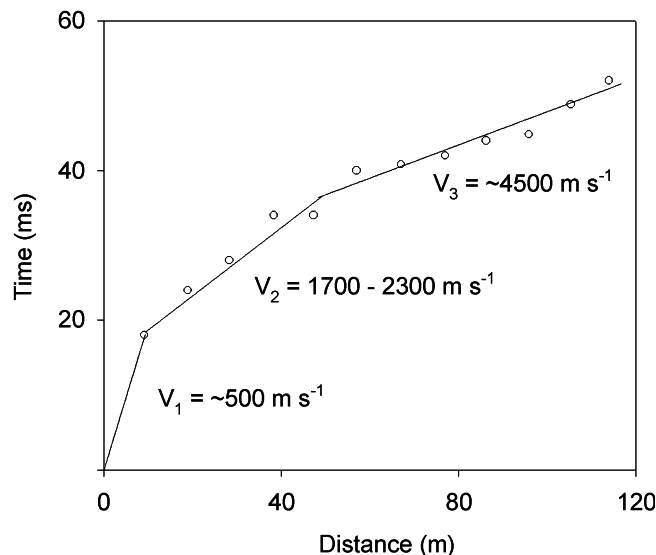


Fig. 2. P-wave first arrival times from an array along the main-trunk center line. Layer 1 is the debris mantle; layers 2 and 3 may represent a discontinuity within the ice–rock mixture. $V_i = (\text{slope of linear segments})^{-1}$.

GEOPHYSICAL METHODS AND RESULTS

Seismic surveys

We attempted seismic reflection and refraction soundings using a 12-channel Bison[®] digital seismograph with geophone spacing of 7–15 m. For sources we used 300- to 500-grain blank shotgun shells discharged within the debris mantle just below the surface. Geophones were placed in small pits and sandwiched between flat rocks in an attempt to reduce noise. Shots were made at various positions along and off the ends of transverse and longitudinal arrays.

No obvious reflections were identified, probably because of poor source coupling and a low signal-to-noise ratio. We suspect that larger explosive sources may have penetrated the debris mantle more effectively. However, refraction analysis (Fig. 2) indicated a consistent pattern of first arrivals and suggested the presence of three layers. Three longitudinal arrays on the main trunk and one on the middle tributary indicated a debris-mantle seismic velocity of 400–500 m s⁻¹, with the second and third layers having velocities of about 1700–2300 and about 4500 m s⁻¹, respectively (Fig. 2). We estimate a debris-mantle thickness of 2–4 m, which is similar to that observed by Elconin and LaChapelle (1997) in moulins and crevasses. We estimate the depth of the second discontinuity to be about 14–23 m. Extrapolations of valley-wall geometry suggest that the base of this second layer represents a discontinuity within the rock glacier, rather than the contact of valley bottom or the valley walls. This is discussed further in Bucki and Echelmeyer (2004). However, the difficulty experienced with source/geophone coupling at the debris mantle precludes detailed resolution of subsurface structure, including the basal layer.

Radio-echo sounding

Thirty ice radar soundings were made with an avalanche-style radio-echo sounder (Watts and England, 1976). The antennas were orientated perpendicular to flow, with a spa-

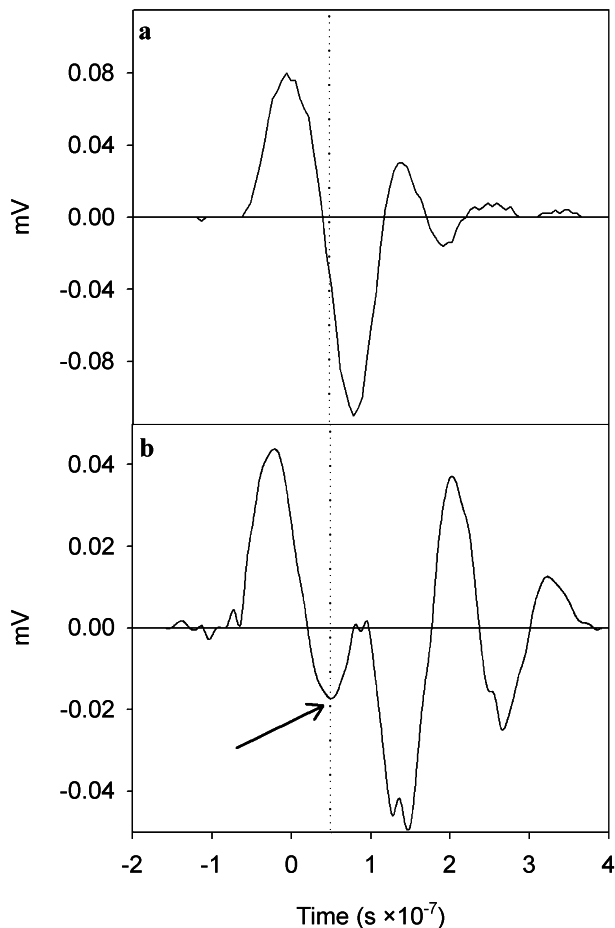


Fig 3. Examples of RES: (a) an airwave with no return signal; (b) interference of the return signal and the airwave creates a distorted signal. (For a deeper rock glacier the return signal would occur after the airwave in each of these panels.) Travel times are determined by measuring the point that the airwave begins to distort as shown by the arrow in (b).

cing of 30–50 m. The observed waveforms showed a distorted signal that appears to be caused by the overlap of the airwave and a return wave (Fig. 3). Such a waveform is typically observed when sounding a very shallow ice glacier. Because of this interference, it was difficult to determine the return signal. However, in some cases we were able to estimate the travel time of the first return, typically in the range 0.12–0.29 μs . Using an electromagnetic wave velocity of 170 $\text{m } \mu\text{s}^{-1}$ (clean ice; Petrenko and Whitworth, 1999) we obtained a reflector “depth” of 10–25 m. These possible returns were not observed everywhere and exhibited no obvious spatial relationship, so they were not used to define rock-glacier geometry.

Electrical methods

There are various electrical resistivity methods that can be used to investigate the subsurface of a rock glacier. We used both d.c. resistivity and TEM, which is an electrical induction method, to investigate Fireweed rock glacier. To aid in our interpretation of these soundings, we made laboratory measurements of the electrical resistivity of rock samples from the debris mantle and others inferred to underlie the main trunk. Our sampling indicates the debris mantle on the west flow contains 80% intrusive rock, much of which is thermally altered. The mantle of the middle flow contains equal amounts of intrusive rocks and mudstone, and the

Table 1. Resistivities of rock types on rock glacier

Sample	Resistivity Ωm
Mudstone 1 (altered)	2024
Mudstone 2	3532
Igneous	3005
Altered igneous 1	910
Altered igneous 2	685
Stream water	8500
Glacier ice (temperate)	$(2.0 \times 10^6) - (1.2 \times 10^8)$

mantle on the east flow comprises two distinct sections. These sections vary in their amounts of intrusive rocks and mudstone; the easternmost part of this flow contains less of the thermally altered rock. We note that these compositions may not represent the relative concentrations of these rock types within the ice–rock mixture.

Electrical properties of rock types

Electrical resistivities of each sample were measured in a laboratory using conventional time-domain methods (Zonge Engineering; Table 1). The altered intrusive rocks had quite low resistivities ($\sim 800 \Omega\text{m}$), while the non-altered igneous rocks and both mudstones had higher resistivities ($>2000 \Omega\text{m}$), similar to those measured by Keller (1991). We also determined the resistivity of the periglacial stream water. It was quite high ($\sim 8500 \Omega\text{m}$), which indicates that it does not contain significant amounts of dissolved ions. These measured resistivities are likely to be somewhat different than in situ values because of fractures, interstitial fluids and water flowing within the rock glacier, so we use them only as guidelines when interpreting our geophysical data.

Direct-current resistivity

Most often used in rock-glacier surveys are d.c. resistivity methods (Fisch and others, 1977; Evin and others, 1997; Hauk, 2001; Vonder Mühlh and others, 2001), in which the resistivity structure is determined by applying a voltage between electrodes placed in the substrate. Good electrical contact between these electrodes and the substrate is important for this technique. This can be limiting on rock glaciers because the electrodes must be placed in the coarse and often dry, unconsolidated debris mantle. On Fireweed rock glacier we attempted d.c. resistivity measurements with dipole–dipole arrays (Reynolds, 1997). In order to overcome the sensitivity that this array type has to electrode contact resistance (Hauck, 2001) we used brine-soaked sponges at each electrode. In spite of these efforts we did not acquire any interpretable data.

Transient electromagnetic (TEM) methods

TEM methods can be used to determine resistivity distribution at depth by measuring the decay of an induced magnetic field (Nabighian, 1979; Kaufman and Keller, 1983; Nabighian and Macnae, 1991). These methods are not often used in glaciology but have been used in permafrost studies and on a few rock

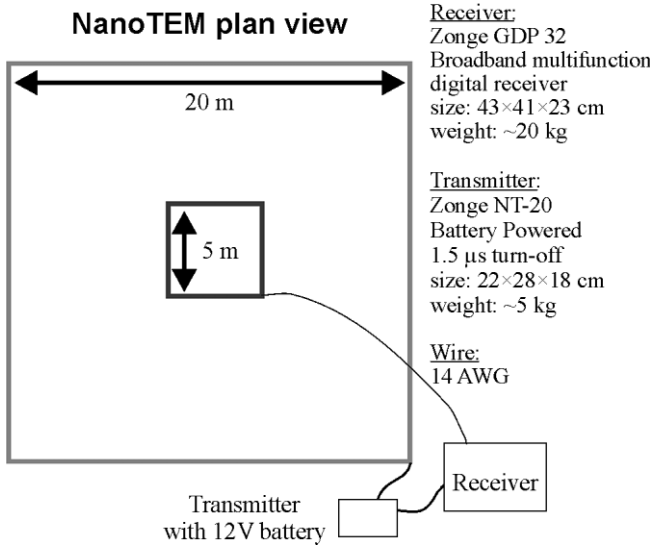


Fig. 4. Array geometry used in our survey (NanoTEM®, Zonge Engineering), which collects a series of data at 31 progressive time windows per measurement, and 400–1000 individual measurements (made at 32 Hz) stacked to compose a sounding. For each measurement, data collection begins at about 1.5 μs and extends to 3 ms after transmitter turn-off.

glaciers (Hauck, 2001; Hauck and others, 2001). Here we provide a brief summary of the basic principles of this method.

Unlike d.c. methods, TEM uses an inductive source and does not require direct electrical-current injection into the debris mantle. Applying a current to a TEM transmitting loop generates a primary magnetic field. Abruptly shutting off this transmitter-loop current induces currents in the substrate. These induced currents generate secondary magnetic fields that decay in proportion to the electrical resistivity of the substrate. These decaying secondary magnetic fields are measured with a receiver loop while the transmitter current is off; the geometry used in this study is shown in Figure 4.

The effective depth of investigation for TEM sounding depends on the size of the transmitter loop, background noise and resistivity of the substrate. The rate at which the current can be shut off in the transmitter loop prior to measurements is a limiting factor in resolving shallow depths. Rock glaciers can be considered shallow in the context of TEM soundings and we are interested in near-surface structure, so rapid termination of the transmitter current is required. Systems that employ such a rapid turn-off (~1.5 μs) are capable of depth resolution of a few meters, even in resistive substrates such as ice.

It has been shown by Nabighian (1979) that the combined effect of all induced currents in a uniform half-space can be approximated by a single current filament moving downward with a velocity v given by

$$v = \left(\frac{4\rho}{\pi\mu t} \right)^{\frac{1}{2}}, \tag{1}$$

where ρ is the resistivity of the half-space, μ is its magnetic permeability and t is the time since the turn-off of the primary magnetic field. This current filament expands like a “smoke ring” downward at an angle of 35–45° from the transmitter loop. In a layered half-space the current filament moves with varying velocity as it crosses layer boundaries. If it encounters a layer with a very low resistivity, its velocity is reduced (Nabighian and Macnae, 1991). ATEM sounding is a

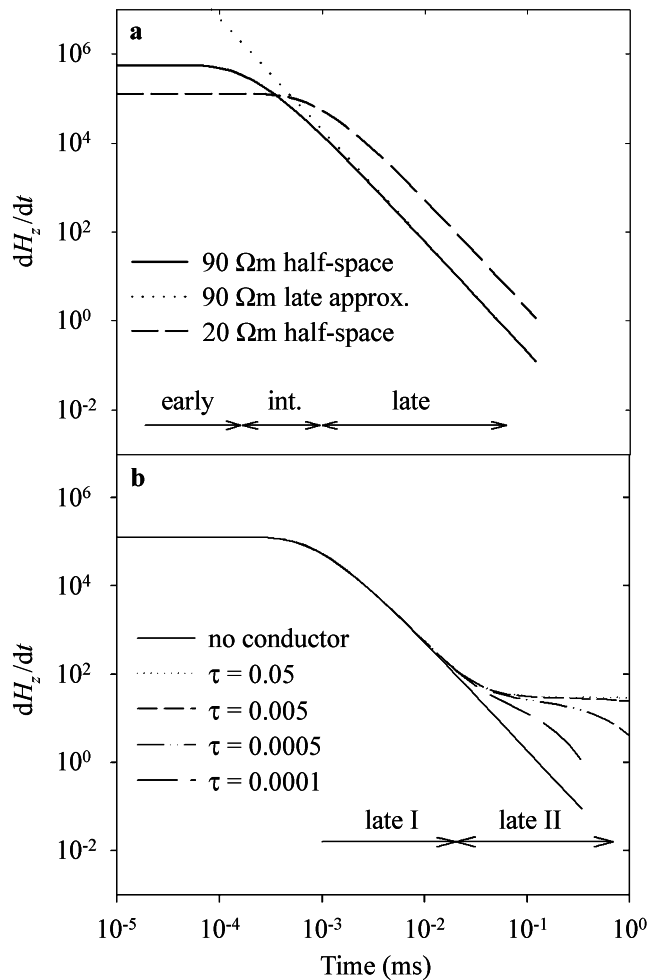


Fig. 5. Time rate of change of the secondary magnetic field is measured (dH_z/dt) vs time from the shut-off of the primary magnetic field. (a) Responses from two half-spaces after Kaufman (1979) with an 11 m transmitter radius and current of 3.5 A. “Early”, “intermediate” and “late” correspond to decay stages and are shown for the 90 Ωm half-space. (b) Complete response in the presence of a conductor can be modeled as the superposition of a power-law response from a half-space and the exponential response of a conductor (Equations (2) and (3)). Late time is divided into late time I and late time II.

measurement of the time rate of change of the secondary magnetic field generated by this downward-propagating “smoke ring”.

Kaufman (1979) gives the response for a circular in-loop array at the surface of a uniform half-space. This is shown in Figure 5a for a transmitter with radius 11 m and a current of 3.5 A. The transient response can be divided into three stages: early time, intermediate time and late time. In the early time the rate of change of the magnetic field is nearly constant, with a value that is proportional to the resistivity of the half-space (early-time segment in Fig. 5a). Intermediate time is the transition from early time to late time. The resistivity of the half-space influences how quickly this transition is made. This is also illustrated in Figure 5a, where two half-spaces having 90 and 20 Ωm resistivities are compared. At late time the transient response can be approximated as

$$\frac{\partial H_z}{\partial t} \approx A_0 \frac{I}{\rho^{\frac{2}{3}}} t^{-k}, \tag{2}$$

where $k = 2.5$ for a uniform half-space, as shown in Figure 5,

while for a layered geology k can vary from about 1.5 to 3.5. A_0 encompasses physical constants and geometry. Changes in the slope of the transient-decay curve can be used to infer the presence of layers of different resistivity. However, the relationship is not unique.

At some point in time, the secondary magnetic fields decay to background noise levels. This causes increased scatter and a leveling in the TEM transient curves (Fig. 5a). However, this decay to background noise levels is not observed if nearby geology includes a sufficiently low resistivity unit, i.e. a “conductor”. In the context of TEM modeling, one-dimensional (1-D) means a model with horizontal layers. Two-dimensional (2-D) means a model of geologic structure with arbitrary variation in cross-section, but no variation along strike. Three-dimensional (3-D) modeling incorporates arbitrary variation both in cross-section and along strike. Two-dimensional conductive bodies, such as cylinders or slabs with infinite strike extent, and 3-D conductive bodies, such as spheres or rectangular block-shaped geologic features, generate an exponentially decaying secondary field (Equation (3)) rather than the power-law decay characteristic of the half-space (Equation (2)).

$$\frac{\partial H_z}{\partial t} \approx A_1 e^{-t/\tau}, \quad (3)$$

where A_1 encompasses geometric parameters and τ is the characteristic time of the conductor. The characteristic time contains information on the dimensions and resistivity of the conductive object (Nabighian and Macnae, 1991). When a conductive body is situated within a half-space, the TEM decay curve has contributions from both the half-space and the conductor. A conductor within a resistive half-space can be recognized if its response is sufficiently strong relative to background. To illustrate this, Equations (2) and (3) can be superimposed, as shown in Figure 5b for various values of τ and $A_1 = 30$. Here, we distinguish between two stages: late time I and late time II. In late time I the TEM transient follows a power law (Equation (2)). In late time II the transient decays into background noise levels or, if a conductive body is present, has an exponential late-time decay (Equation (3)).

Transient-decay curves contain a significant amount of detail about the subsurface resistivity structure; however, this structure is not necessarily directly apparent. To more clearly express the resistivity structure of the subsurface, the transient-decay curves can be re-parameterized into resistivity–depth curves through inversion. Converting the decay curve into either an apparent resistivity curve or a smoothly varying resistivity model improves the expression of geologic structure. Apparent resistivity curves are determined by fitting a uniform half-space response (Kaufman and Keller, 1983) to each data point of the transient-decay curve. Smooth-model inversion assumes a horizontally layered resistivity structure and solves for a model of resistivities that vary smoothly from layer to layer and that generates a calculated transient-decay curve that matches the measured data as closely as possible (Ward and Hohmann, 1987). This later approach can provide more detail about the subsurface than apparent resistivity calculations because it uses a more complete model of subsurface resistivity. Smooth-model resistivities are based on a complete solution to the layered-earth TEM response, and they provide more realistic values of the true resistivity structure than apparent resistivity curves. Alternatively, a

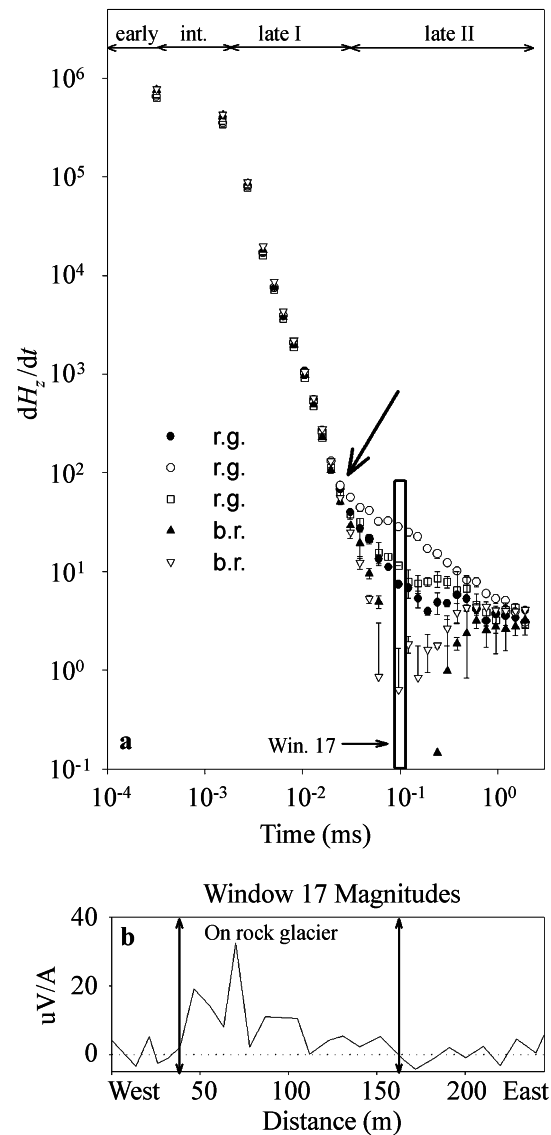


Fig. 6 (a). Decay curves from the transverse transect; three soundings are from on the rock glacier (r.g.) and two are from on the bedrock (b.r.). Error bars reflect the standard deviations of the stacked records in each case. A relatively slow decay after the arrow occurs in many of the r.g. soundings, but not for those soundings on b.r. The slow decay is characteristic of a conductor. (b) Shows how this conductive response varies along the transverse transect. We use window 17 (indicated in (a) as “Win. 17”) for all soundings in this transect. Plotting the magnitude graphically shows how the conductive response varies across the rock glacier. It is interesting to note that the strongest response is offset to the west.

layered inversion with fewer layers but with no restrictions on resistivity changes between layers can be used. This type of inversion allows specification of the number of layers, layer resistivity and layer thickness. Zonge Engineering developed the inversion software used in this study. Modeling results from a transect of soundings can be plotted as a pseudo-section showing contours of resistivity vs distance along line and depth from surface.

Errors in TEM measurements occur if there are deviations from the assumed shape and relationship of the transmitter and receiver loops. For this reason, it is important to maintain consistent loop geometries throughout a survey. Topographic effects can also introduce error in TEM soundings, but accounting for the relative position of each sounding reduces these errors.

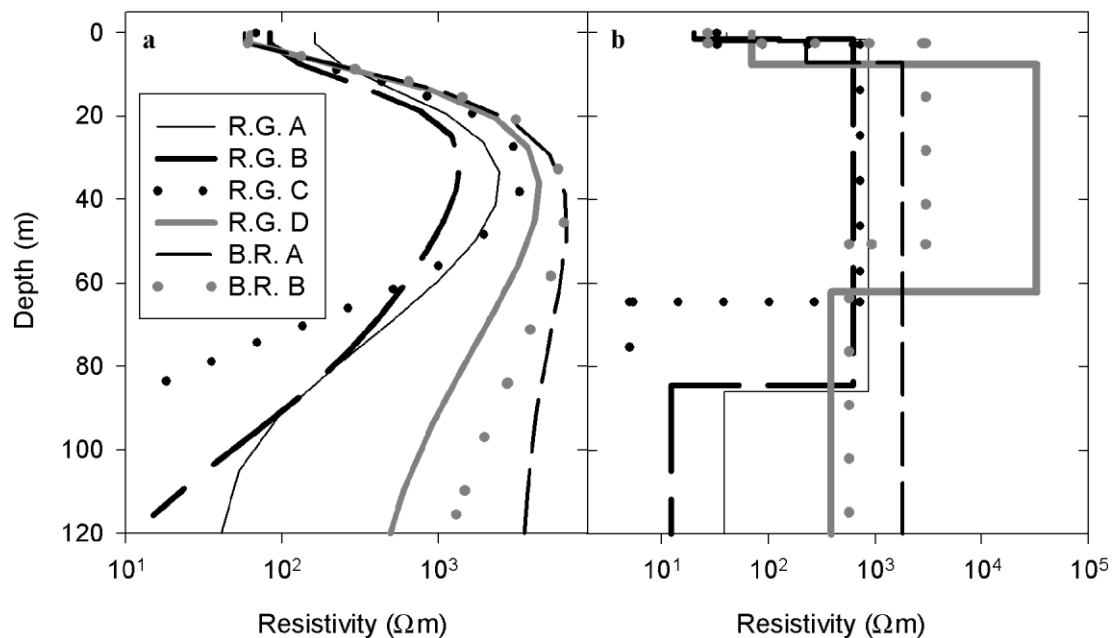


Fig. 7 (a). Smooth-model inversions of rock-glacier soundings (R.G. A–D) and bedrock soundings (B.R. A and B). (b) Three-layer inversions for the same soundings as those in (a). Layered inversions are typically used for picking depths when geology is 1-D.

Summarizing the expected structure of the TEM transient-decay curves, we note there are several key features. The nearly constant level of the early phase and its duration give some information about the overall resistivity of the upper layers. A change in the slope of the late-time I stage represents resistivity changes with depth, whereas the late-time II stage can indicate the presence of conductive geologic features following Equation (3). These guidelines apply when 1-D assumptions are valid. We note that 2-D and 3-D structures can influence any portion of the curve.

TEM data

Ten soundings were performed along the center line of the main trunk (Fig. 1b). The first sounding was made about 120 m up-glacier from the terminus, and subsequent soundings extended to the uppermost main trunk. An additional 30-sounding transect was made across the main trunk and included soundings off the rock glacier on or near bedrock exposures. This transect crossed the main trunk about 150 m up-valley (Fig. 1b). Figure 6a shows three typical decay curves from the rock glacier and two from the bedrock.

Discussion of TEM results

The decay curves in Figure 6a are, at first viewing, quite similar to each other, especially for times before late II. Close examination of the late II times highlights differences that represent variations in resistivity structure between the bedrock and the rock glacier. At these times, the bedrock curves rapidly become noisy, whereas the rock-glacier curve shows a characteristic exponential decay (Equation (3)). This slow, less noisy decay is observed in all curves from the center-line profile and in most curves taken on the rock glacier from the transverse profile. This behavior suggests that there is a conductive feature within, on or under the rock glacier that is not present in the bedrock. To illustrate this we have plotted the magnitudes of window 17 (the data point at approximately 0.1 ms in Fig. 6a) for all soundings in

the transverse profile (Fig. 6b). This window (and most others in late II) is near zero and sometimes negative for soundings taken off the rock glacier. However, for those soundings on the rock glacier (between vertical arrows in Fig. 6b) this window is always positive and often high-magnitude. Figure 6b shows how the conductive response varies across the rock glacier and that there are distinctions among soundings off and on the rock glacier. We note that the low-resistivity response is greatest just to the west of the center line.

One-dimensional smooth-model and layered inversions are used to determine subsurface resistivity structures (Fig. 7). Both types of inversion techniques show the same basic resistivity structure for the rock glacier and the same for the bedrock. The rock-glacier soundings (R.G. A–D, Fig. 7) consistently show a surface layer a few meters thick with resistivity values near 100–300 Ωm . This layer overlies a more resistive region that is 60–70 m thick and $\geq 1000 \Omega\text{m}$. The inversions for most of the rock-glacier soundings are clearly distinguished from bedrock soundings by a low-resistivity structure that underlies the highly resistive region (compare R.G. A–C with B.R. A and B). The resistivity of this structure does vary among the rock-glacier soundings. For example, R.G. C in Figure 7a shows a much lower resistivity at depth than R.G. D. The modeled structure in R.G. D is of higher resistivity than the other rock-glacier soundings but it is still an order of magnitude lower than the bedrock resistivity at depth. These model results are consistent with what would be expected from the raw data (Fig. 6) and our preliminary analysis above.

Figure 7b shows 1-D layered inversions for the same soundings as in Figure 7a. In a layered inversion the number of layers is fixed and the inversion is used to solve for thickness and resistivity. In Figure 7b, horizontal line segments represent the contacts of these layers. Based on our smooth models (Fig. 7a) we used a three-layer model to represent an upper layer, which is perhaps the debris mantle, a second layer thought to be an ice–rock mixture, and a third, lowermost layer, for which resistivities and

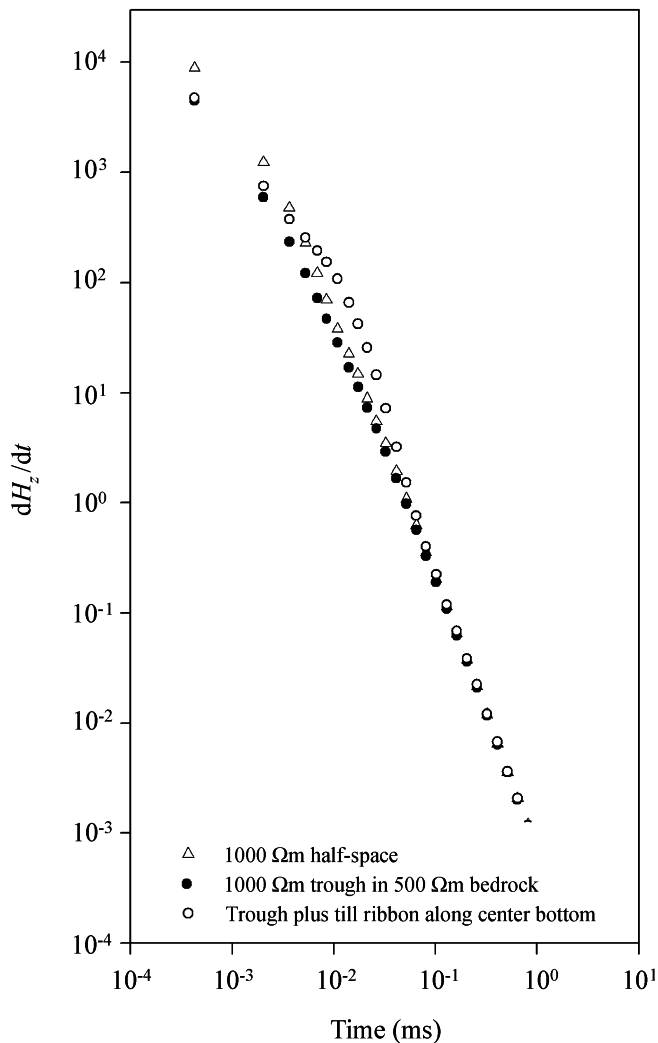


Fig. 8. Two-dimensional forward models. A simple half-space, a channel and a channel with a conductive till at the bottom center.

thickness were not assigned. Layered inversions produced the same basic resistivity structure as the smooth models but provide an estimate of layer thickness and rock-glacier depth. For most of the rock-glacier soundings, the debris-mantle thickness is well resolved through the layered-inversion method and is similar to that determined with seismic methods (2–4 m; Fig. 2).

The conductive structure ($< 80 \Omega\text{m}$) at depth is evident in most of the rock-glacier inversions, but is not evident in the bedrock inversions. This conductive structure is thought to represent a till-like layer. Elconin (1995) described the existence of a < 2 m thick wet mud layer between the bed of the rock glacier and the bedrock. He describes an exposure of this material between the eastern bedrock wall and the rock glacier as containing mostly clay-, silt- and sand-size material with angular clasts 5–150 mm in diameter. The material is described as being colored yellow, red and orange-brown, with a fetid odor. Elconin (1995) notes the presence of alder roots oriented in the direction of flow, which may indicate deformation within this layer. This mud may be analogous to a deformable subglacial till (e.g. Paterson, 1994). It was also reported that within the rock-glacier/ice-rock mixture there was significant silt and clay (Elconin and LaChapelle, 1997). From these observations, it is quite likely that there exists a significant amount of wet, fine-grained material beneath the rock glacier. However, some

of the geophysical evidence and the analysis of rock-glacier motion (Bucki and Echelmeyer, 2004) seems to indicate that a shear plane exists at 20–28 m depth where most of the motion of the rock glacier probably occurs.

It is unlikely that this conductive response at depth is the result of a different type of bedrock found under the rock glacier than along its margins. The conductive response could also represent water-saturated bedrock or water flowing under the rock glacier. However, if this is the case, then this water must not be connected to the highly resistive water flowing in the periglacial stream (Table 1).

The modeled depth for the till-like layer near the terminus is deeper than the thickness of the rock glacier measured at the terminus exposure (58 m). This suggests that our layered inversions produce an overdeepened depth-to-bed model. This may be a result of applying a 1-D model to a TEM response of a 2- or 3-D feature. To investigate this we used a 2-D TEM forward model (Rijo and Hohmann, 1999; Zonge Engineering) to calculate a TEM response over the center of a hypothetical rock-glacier-filled channel. Figure 8 shows the expected responses for a simple $1000 \Omega\text{m}$ half-space, a $1000 \Omega\text{m}$ channel within a $500 \Omega\text{m}$ bedrock half-space and this same channel with a ribbon of till situated at the bottom of the channel. These 2-D features create significant deflections from the simple half-space model (Fig. 8) at early times. Using the forward modeling results for the channel plus the till model, we used the 1-D inversion to reconstruct the resistivity. We found that the 1-D inversion successfully recovers the low-resistivity feature but places it at a greater depth. This is consistent with our observations near the terminus and we expect that it would be true for all the soundings up the center line of the rock glacier, since the entire main trunk seems to be situated within a trough (Bucki and Echelmeyer, 2004).

We cannot reliably use layered inversions to determine rock-glacier depth because of the negative 2-D effects discussed above. Instead, we use the measured 58 m thickness at the terminus to calibrate the smooth-model inversion of the nearest terminus center-line sounding. This calibration defines the “depth to till”, which we specify to be $\sim 900 \Omega\text{m}$. This calibration is then extended up-glacier for the remainder of the center-line soundings. We note that the resolution of the basal discontinuity is limited by the averaging effect of the smooth-model inversion. To pick the depth, we use the depth that corresponds to the $900 \Omega\text{m}$ level in all of the soundings.

The smooth-model inversions for each of the ten soundings along the center line are plotted along section in Figure 9a, where the location of each sounding is shown along the top axis. The data are then contoured to produce a pseudo-section along the rock glacier from about 120 m to 530 m up from the terminal face (located at 0 m), which we interpret as an approximate profile of rock-glacier thickness. This profile shows structure in the basal topography that is similar to that observed in the surface topography and marginal features. For example, Figure 1 shows the location of two snow-filled depressions along the margins (“D”), where we might expect a deeper rock-glacier bed. There is a corresponding depression in the pseudo-section at a longitudinal position of 340 m (“D” in Fig. 9a), and a corresponding change in surface slope, consistent with a rock glacier flowing over a dip in its bed.

From the center-line profile data, the corresponding thickness and the slope of the valley walls, it is possible to

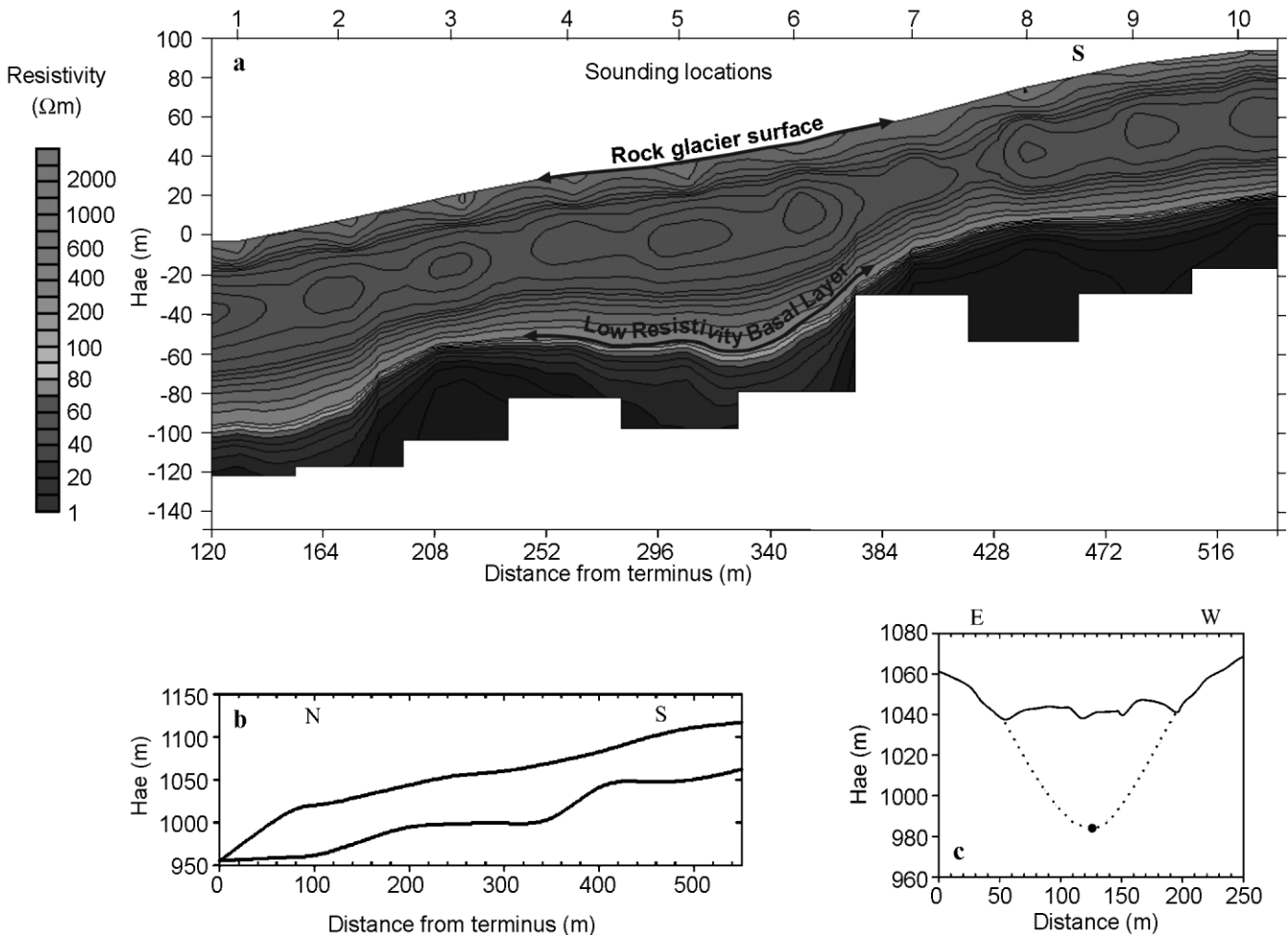


Fig. 9 (a). NanoTEM smooth-model resistivity cross-section; “D” corresponds to the feature marked with the same letter in Figure 1b. (b) Center-line profile determined from NanoTEM soundings by methods described in the text. (c) Transverse parabolic cross-section 170 m from terminus, determined from surface topography and center-line NanoTEM depth. Parabolic geometry is inferred. Hae is height about the ellipsoid.

construct an approximate transverse cross-section that conforms to reasonable channel geometry, as shown in Figure 9c. We do know through observations at the terminus (Bucki, 2002; Bucki and Echelmeyer, 2004) that the actual channel geometry may be slightly asymmetrical, where the deepest part is actually offset to the west.

CONCLUSIONS

We have investigated the geometry of Fireweed rock glacier using various geophysical techniques. TEM methods yield the best results for the complex geometry of this rock glacier. The instrumental set-up and data collection of TEM methods are efficient, require minimal time and they effectively circumvent the debris-mantle coupling problems that complicate other geophysical methods. Direct-current resistivity and seismic reflection methods were of limited value. Using seismic refraction, we were able to resolve the thickness of the low-velocity debris mantle (2–4 m). This thickness was also determined using a layered inversion of the TEM data and is consistent with direct observations made by Elconin and LaChapelle (1997).

The highlight of TEM is the ability to resolve rock-glacier thickness along the main trunk (40–60 m) and detect a sub-rock-glacier conductive feature, but the ability to determine thickness may be dependent on the presence of

this conductive feature. Additionally, the modeled depth of this feature is subject to influences of 2-D and, quite likely, 3-D structures (Figs 7 and 8), which tend to deepen the 1-D modeling results. Calibration of smooth models with the terminus exposure allows us to develop an approximate longitudinal profile along the main trunk (Fig. 9b), and the slope of the valley walls was used to construct an approximate transverse cross-section (Fig. 9c).

We expect that the conductive feature is similar to a sub-glacial till. The TEM response of this “till” varies across the transverse profile (Fig. 6b), and this variability may reflect spatial variations in till thickness and/or resistivity. It is interesting that the geometry of the terminus described in Bucki (2002) and Bucki and Echelmeyer (2004) is asymmetrical, and the same asymmetry is observed in TEM soundings (Fig. 6b), where the deepest/most conductive region is offset to the west.

Additionally, seismic refraction and, to a lesser extent, RES suggest a discontinuity at about 18–28 m depth within the rock glacier. Such a discontinuity may also be suggested by the TEM smooth-model results at about 20 m depth (Fig. 7a), but layered inversions indicate that this may be the result of the inherent smoothing of that method. Analysis of the observed surface motion by Bucki and Echelmeyer (2004) showed that the distribution of velocities across the rock glacier is more consistent with flow through a shallow pseudo-rectangular channel than with flow

through a deeper valley-shaped channel. That study indicates that the discontinuity observed here with the geophysical methods may be a “shear plane” at depth, on and above which most of the motion occurs. It is interesting that the “basal till” is not associated with this shear plane. The motion of ice glaciers is typically concentrated at depth near the bed and may often include motion within a subglacial till (e.g. Paterson, 1994). This does not seem to be the situation for this rock glacier, where a “till” exists near the bed but the motion is likely concentrated well above it (Bucki and Echelmeyer, 2004).

ACKNOWLEDGEMENTS

This study was supported by U.S. National Science Foundation grant No. NSF-OPP98 06648. We would like to thank D. Rosenkrans and the National Park Service for cooperation and support, and K. Zonge and S. Urquart (Zonge Engineering and Research, Inc., Tucson, AZ) for their invaluable assistance with the electrical methods. We appreciate the contributions of C. Bucki, L. Cox, P. Del Vecchio, R. Elconin, L. Goodman, W. Harrison, D. Mouldry, K. Smith, M. Truffer and E. Wescott. K-9 support throughout this project was provided by Tazlina, Choly, Baxter and McKenzie. We would like to thank J. Degenhardt and an anonymous reviewer for their hard work that helped improve this contribution.

REFERENCES

- Berthling, I., B. Etzelmüller, K. Isaksen and J. L. Sollid. 2000. Rock glaciers on Prins Karls Forland. II: GPR soundings and the development of internal structures. *Permafrost and Periglacial Processes*, **11** (4), 357–369.
- Bucki, A. K. 2002. Geometry and flow of Fireweed Rock Glacier, Alaska. (M.Sc. thesis, University of Alaska Fairbanks.)
- Bucki, A. and K. A. Echelmeyer. 2004. The flow of Fireweed rock glacier, Alaska, U.S.A. *J. Glaciol.* **50**(168), 76–86.
- Costello, D. P. 2000. Seismic and geomorphic investigations of Galena Creek Rock Glacier. (M.Sc. thesis, University of Colorado, Boulder.)
- Degenhardt, J. J., Jr and J.R. Giardino. 2003. Subsurface investigation of a rock glacier using ground penetrating radar (GPR): implication for locating stored water on mars. *J. Geophys. Res.*, **108** (E4), 8036.
- Degenhardt, J. J., Jr, J. R. Giardino, M. B. Junck, M. P. Quntana and R. A. Marston. 2000. Evaluating the internal structure of a rock glacier using ground penetrating radar (GPR): Yankee Boy Basin, CO, U.S.A. *Geol. Soc. Am. Abstr. Programs*, **32**(7), A516.
- Elconin, R. F. 1985. Internal composition, structure, and genesis of an active and well developed compound rock glacier, Wrangell Mountains, Alaska. (M.Sc. thesis, Humboldt State University, Arcata, CA.)
- Elconin, R. F. and E. R. LaChapelle. 1997. Flow and internal structure of a rock glacier. *J. Glaciol.*, **43**(144), 238–244.
- Evin, M., D. Fabre and P. G. Johnson. 1997. Electrical resistivity measurements

- on the rock glaciers of Grizzly Creek, St. Elias Mountains. *Permafrost and Periglacial Processes*, **8**(2), 179–189.
- Fisch, W., Sr, W. Fisch, Jr and W. Haerberli. 1978. Electrical D.C. resistivity soundings with long profiles on rock glaciers and moraines in the Alps of Switzerland. *Z. Gletscherkd. Glazialgeol.*, **13**(1–2), [1977], 239–260.
- Haerberli, W. 1985. Creep of mountain permafrost: internal structure and flow of Alpine rock glaciers. *Eidg. Tech. Hochschule, Zürich. Versuchsanst. Wasserbau, Hydrol. Glaziol. Mitt.* 77.
- Hauck, C. 2001. Geophysical methods for detecting permafrost in high mountains. *Eidg. Tech. Hochschule, Zürich. Versuchsanst. Wasserbau, Hydrol. Glaziol. Mitt.* 171.
- Hauck, C., M. Guglielmin, K. Isaksen and D. Vonder Mühl. 2001. Applicability of frequency domain and time-domain electromagnetic methods. *Permafrost and Periglacial Processes*, **12**(1), 39–52.
- Isaksen, K., R.S. Ødegård, T. Eiken and J. L. Sollid. 2000. Composition, flow and development of two tongue-shaped rock glaciers in the permafrost of Svalbard. *Permafrost and Periglacial Processes*, **11** (3), 241–257.
- Kääb, A., W. Haerberli and G. H. Gudmundsson. 1997. Analysing the creep of mountain permafrost using high precision aerial photogrammetry: 25 years of monitoring Gruben rock glacier, Swiss Alps. *Permafrost and Periglacial Processes*, **8**(4), 409–426.
- Kaufman, A. A. 1979. Harmonic and transient fields on the surface of a two-layer medium. *Geophysics*, **44**(7), 1208–1217.
- Kaufman, A. A. and G. V. Keller. 1983. *Frequency and transient soundings*. New York, Elsevier.
- Keller, G.V. and G.W. Hohmann. 1991. Rock and mineral properties. In Nabighian, M.N., ed. *Electromagnetic methods in applied geophysics Vol. 2. Application*. Tulsa, OK, Society of Exploration Geophysicists, 13–51. (Monograph 12.)
- Konrad, S. K. and N. F. Humphrey. 2000. Steady-state flow model of debris-covered glaciers (rock glaciers). *International Association of Hydrological Sciences Publication 264* (Symposium at Seattle 2000—*Debris-Covered Glaciers*), 255–263.
- MacKevett, E. M. and J. G. Smith. 1972. *Geologic map of the McCarthy B-6 Quadrangle, Alaska*. Reston, VA, U.S. Geological Survey. (USGS Quadrangle Map GQ-1035.)
- Nabighian, M. N. 1979. Quasi-static transient response of a conducting half-space — an approximate representation. *Geophysics*, **44**, 1700–1705.
- Nabighian, M.N. and J. C. Macnae. 1991. Time-domain electromagnetic prospecting methods. In Nabighian, M.N., ed. *Electromagnetic methods in applied geophysics. Vol. 2. Application*. Tulsa, OK, Society of Exploration Geophysicists, 427–478. (Monograph 12.)
- Paterson, W. S. B. 1994. *The physics of glaciers. Third edition*. Oxford, etc., Elsevier.
- Petrenko, V. F. and R. W. Whitworth. 1999. *Physics of ice*. Oxford, etc., Oxford University Press.
- Reynolds, J. M. 1997. *An introduction to applied and environmental geophysics*. Chichester, John Wiley and Sons.
- Rijo, L. and J. Hohmann. 1999. TEM2D v1.0. Salt Lake City, University of Utah. College of Mines and Earth Sciences.
- Vonder Mühl, D., C. Hauck, H. Gubler, R. McDonald and N. Russill. 2001. New geophysical methods of investigating the nature and distribution of mountain permafrost with special reference to radiometry techniques. *Permafrost and Periglacial Processes*, **12**(1), 27–38.
- Ward, S. H. and G. W. Hohmann. 1987. Electromagnetic theory for geophysical applications. In Nabighian, M.N., ed. *Electromagnetic methods in applied geophysics Vol. 1. Theory*. Tulsa, OK, Society of Exploration Geophysicists, 131–313. (Monograph 3)
- Watts, R. D. and A.W. England. 1976. Radio-echo sounding of temperate glaciers: ice properties and sounder design criteria. *J. Glaciol.*, **17**(75), 39–48.

MS received 11 May 2002 and accepted in revised form 5 January 2004